articles

molecular pharmaceutics

MRI-Visible Micellar Nanomedicine for Targeted Drug Delivery to Lung Cancer Cells

Jagadeesh Setti Guthi,[†,‡] Su-Geun Yang,[†,‡] Gang Huang,[†] Shunzi Li,[†,§] Chalermchai Khemtong,[†] Chase W. Kessinger,[†] Michael Peyton,[†,||] John D. Minna,[†,§,||] Kathlynn C. Brown[†,§], and Jinming Gao*[,†]

Department of Pharmacology, Simmons Comprehensive Cancer Center, Department of Internal Medicine, Division of Translational Research, and Hamon Center for Therapeutic Oncology Research, University of Texas Southwestern Medical Center at Dallas, Dallas, Texas 75390

Received May 22, 2009; Revised Manuscript Received August 17, 2009; Accepted August 26, 2009

Abstract: Polymeric micelles are emerging as a highly integrated nanoplatform for cancer targeting, drug delivery and tumor imaging applications. In this study, we describe a multifunctional micelle (MFM) system that is encoded with a lung cancer-targeting peptide (LCP), and encapsulated with superparamagnetic iron oxide (SPIO) and doxorubicin (Doxo) for MR imaging and therapeutic delivery, respectively. The LCP-encoded MFM showed significantly increased $\alpha_v\beta_6$-dependent cell targeting in H2009 lung cancer cells over a scrambled peptide (SP)-encoded MFM control as well as in an $\alpha_v\beta_6$-negative H460 cell control. ^{3}H-Labeled MFM nanoparticles were used to quantify the time- and dose-dependent cell uptake of MFM nanoparticles with different peptide encoding (LCP vs SP) and surface densities (20% and 40%) in H2009 cells. LCP functionalization of the micelle surface increased uptake of the MFM by more than 3-fold compared to the SP control. These results were confirmed by confocal laser scanning microscopy, which further demonstrated the successful Doxo release from MFM and accumulation in the nucleus. SPIO clustering inside the micelle core resulted in high T_2 relaxivity (>400 Fe mM^{-1} s^{-1}) of the resulting MFM nanoparticles. T_2-weighted MRI images showed clear contrast differences between H2009 cells incubated with LCP-encoded MFM over the SP-encoded MFM control. An ATP activity assay showed increased cytotoxicity of LCP-encoded MFM over SP-encoded MFM in H2009 cells (IC_{50} values were 28.3 $\pm$ 6.4 nM and 73.6 $\pm$ 6.3 nM, respectively; $p < 0.005$). The integrated diagnostic and therapeutic design of MFM nanomedicine potentially allows for image-guided, target-specific treatment of lung cancer.

Keywords: Polymeric micelles; magnetic resonance imaging; theranostic nanomedicine; doxorubicin; $\alpha_v\beta_6$ integrin; superparamagnetic iron oxide; lung cancer therapy

Introduction

Lung cancer is the leading cause of cancer-related deaths for both men and women in the USA, with 5-year survival rates less than 15%.[1] Current cytotoxic chemotherapy for lung cancer lacks adequate specificity and efficacy, which provides an impetus to develop targeted therapies to achieve greater efficacy with fewer side effects. In recent years, nanomedicine platforms that integrate imaging and therapeutic functions (e.g., image-visible nanotherapeutics) have received considerable attention as the next generation of medicine.[2−6] Unlike traditional small molecular contrast agents or drugs, image-visible nanomedicine has the potential

* Address correspondence to Jinming Gao, Ph.D., Department of Pharmacology, Simmons Comprehensive Cancer Center, UT Southwestern Medical Center, 5323 Harry Hines Blvd., Dallas, TX 75390-8807. Phone: 214-645-6370. Fax: 214-645-6347. E-mail: jinming.gao@utsouthwestern.edu.

† Department of Pharmacology, Simmons Comprehensive Cancer Center.

‡ These authors contribute equally to this work.

§ Department of Internal Medicine, Division of Translational Research.

|| Hamon Center for Therapeutic Oncology Research.

(1) Jemal, A.; Siegel, R.; Ward, E.; Hao, Y.; Xu, J.; Murray, T.; Thun, M. J. Cancer statistics, 2008. *Ca—Cancer J. Clin.* **2008**, *58* (2), 71–96.

(2) Ferrari, M. Cancer nanotechnology: opportunities and challenges. *Nat. Rev. Cancer* **2005**, *5* (3), 161–171.

10.1021/mp9001393
Published on Web 08/26/2009

to provide simultaneous molecular diagnosis and therapeutic treatment in one system. Such integrated diagnostic and therapeutic designs allow for the timely tailoring of nanomedicine modules to address the challenges of tumor heterogeneity and adaptive resistance,[4] which can ultimately help achieve the goal of personalized therapy for lung cancer.

Among the many exciting nanoplatforms such as liposomes and dendrimers, polymeric micelles provide a complementary yet unique nanocarrier system.[7−11] Polymeric micelles are composed of amphiphilic block copolymers that contain distinguished hydrophobic and hydrophilic segments. The distinctive chemical nature of the two blocks results in thermodynamic phase separation in aqueous solution and formation of nanoscopic supramolecular core/shell structures. This unique architecture enables the hydrophobic micelle core to serve as a nanoscopic depot for therapeutic or imaging agents and the shell as biospecific surfaces for targeting applications. Recently, our lab has demonstrated a multifunctional micelle design that allows for the vascular targeting of tumor endothelial cells, MRI ultrasensitivity, and controlled release of doxorubicin (Doxo) for therapeutic drug delivery.[12,13]

In this study, we report the development of MRI-visible polymeric micelles that target lung cancer cells (Figure 1A). The micelle surface was functionalized with a lung cancer-targeting peptide (LCP, aka H2009.1, with a sequence of RGDLATLRQL), which was isolated from a phage-displayed peptide library by biopanning on the lung adenocarcinoma cell line H2009.[14−16] This peptide binds to the restrictively expressed integrin, $\alpha_v\beta_6$, which is upregulated in many human non-small-cell lung carcinomas compared to normal lung tissue.[17] A scrambled peptide (SP, with the same amino acid composition as LCP but a scrambled sequence of DALRLQGTLR) was used as a control. Doxorubicin (Doxo) and superparamagnetic iron oxide (SPIO) were loaded inside the micelle core for therapeutic delivery and MR imaging applications, respectively. In this study, we systematically examined the cell-targeting specificity of LCP-encoded polymeric micelles in $\alpha_v\beta_6$-expressing H2009 lung cancer cells over the $\alpha_v\beta_6$-negative H460 cells as a function of LCP surface density, micelle dose and cell incubation time. The LCP-encoded multifunctional micelles (MFM) demonstrated more sensitive targeted detection by MRI and better therapeutic efficacy in H2009 lung cancer cells over the SP-encoded MFM control. This integrated micellar nanomedicine that combines cancer targeting, MRI visibility and therapeutic delivery functions should contribute to the growing arsenal for targeted therapy of lung cancer.

Materials and Methods

Materials. Doxorubicin (doxorubicin-HCl, 2 mg/mL, in 0.9% NaCl) was purchased from the Bedford Laboratories (Bedford, OH) and was precipitated with addition of triethylamine to obtain the hydrophobic drug. Maleimide-terminated poly(ethylene glycol)-*co*-poly(D,L-lactic acid) (Mal-PEG-PLA, molecular weights of both PEG and PLA segments are 5 kDa) and methoxy-terminated poly(ethylene glycol)-*co*-poly(D,L-lactic acid) (MeO-PEG-PLA, 5 kDa for both segments) were synthesized following previously published procedure.[13,18] Tritium labeled acetyl chloride [^{3}H] was purchased from American Radiolabeled Chemicals Inc. (St. Louis, MO) and was used to label the hydroxyl group of MeO-PEG-PLA-OH at the PLA terminal. Lung cancer

(3) Peer, D.; Karp, J. M.; Hong, S.; Farokhzad, O. C.; Margalit, R.; Langer, R. Nanocarriers as an emerging platform for cancer therapy. *Nat. Nanotechnol.* **2007**, *2* (12), 751–760.
(4) Sumer, B.; Gao, J. Theranostic nanomedicine for cancer. *Nanomedicine* **2008**, *3* (2), 137–140.
(5) Torchilin, V. P. Multifunctional nanocarriers. *Adv. Drug Delivery Rev.* **2006**, *58* (14), 1532–1555.
(6) Khemtong, C.; Kessinger, C. W.; Gao, J. Polumeric nanomedicine for cancer MR imaging and drug delivery. *Chem. Commun. (Cambridge)* **2009**, 3497–3510.
(7) Blanco, E.; Kessinger, C. W.; Sumer, B. D.; Gao, J. Multifunctional micellar nanomedicine for cancer therapy. *Exp. Biol. Med. (Maywood)* **2009**, *234* (2), 123–131.
(8) Croy, S. R.; Kwon, G. S. Polymeric micelles for drug delivery. *Curr. Pharm. Des.* **2006**, *12*, 4669–4684.
(9) Nishiyama, N.; Kataoka, K. Current state, achievements, and future prospects of polymeric micelles as nanocarriers for drug and gene delivery. *Pharmacol. Ther.* **2006**, *112* (3), 630–648.
(10) Sutton, D.; Nasongkla, N.; Blanco, E.; Gao, J. Functionalized micellar systems for cancer targeted drug delivery. *Pharm. Res.* **2007**, *24* (6), 1029–1046.
(11) Torchilin, V. P. PEG-based micelles as carriers of contrast agents for different imaging modalities. *Adv. Drug Delivery Rev.* **2002**, *54* (2), 235–252.
(12) Khemtong, C.; Kessinger, C. W.; Ren, J.; Bey, E. A.; Yang, S. G.; Guthi, J. S.; Boothman, D. A.; Sherry, A. D.; Gao, J. In vivo off-resonance saturation magnetic resonance imaging of alphavbeta3-targeted superparamagnetic nanoparticles. *Cancer Res.* **2009**, *69* (4), 1651–1658.
(13) Nasongkla, N.; Bey, E.; Ren, J.; Ai, H.; Khemtong, C.; Guthi, J. S.; Chin, S. F.; Sherry, A. D.; Boothman, D. A.; Gao, J. Multifunctional polymeric micelles as cancer-targeted, MRI-ultrasensitive drug delivery systems. *Nano Lett.* **2006**, *6* (11), 2427–2430.
(14) Guan, H.; McGuire, M. J.; Li, S.; Brown, K. C. Peptide-targeted polyglutamic acid doxorubicin conjugates for the treatment of alpha(v)beta(6)-positive cancers. *Bioconjugate Chem.* **2008**, *19* (9), 1813–1821.
(15) Oyama, T.; Sykes, K. F.; Samli, K. N.; Minna, J. D.; Johnston, S. A.; Brown, K. C. Isolation of lung tumor specific peptides from a random peptide library: generation of diagnostic and cell-targeting reagents. *Cancer Lett.* **2003**, *202* (2), 219–230.
(16) Li, S.; Lin, M.; Liu, Y.-H.; Sun, X.; McGuire, M. J.; Brown, K. C. Synthesis and characterization of a high affinity alpha(v)beta(6)-specific ligand for in vitro and in vivo applications. *Mol. Cancer Ther.* **2009**, *8*, 1239–1249.
(17) Elayadi, A. N.; Samli, K. N.; Prudkin, L.; Liu, Y. H.; Bian, A.; Xie, X. J.; Wistuba, I. I.; Roth, J. A.; McGuire, M. J.; Brown, K. C. A peptide selected by biopanning identifies the integrin alphavbeta6 as a prognostic biomarker for nonsmall cell lung cancer. *Cancer Res.* **2007**, *67* (12), 5889–5895.
(18) Nasongkla, N.; Shuai, X.; Ai, H.; Weinberg, B. D.; Pink, J.; Boothman, D. A.; Gao, J. cRGD-functionalized polymer micelles for targeted doxorubicin delivery. *Angew. Chem., Int. Ed.* **2004**, *43* (46), 6323–6327.

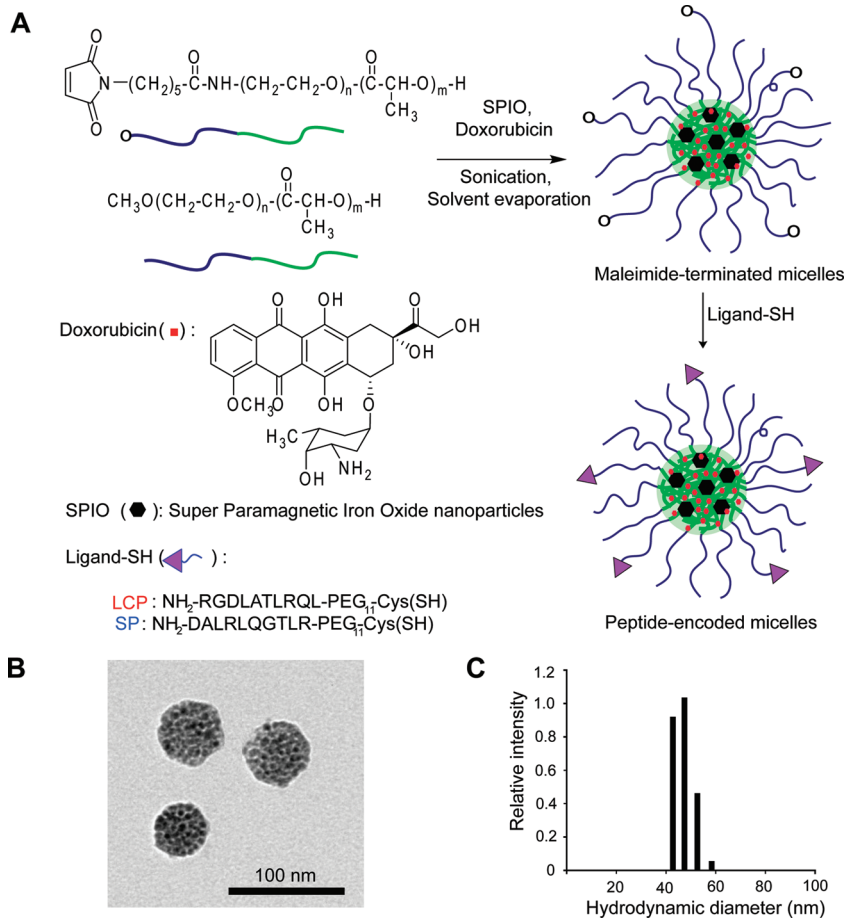

Figure 1. Preparation and physical characterization of multifunctional micelles (MFM) for lung cancer imaging and therapy. (A) Schematic of syntheses of amphiphilic block copolymers and self-assembly of MFM nanoparticles with Doxo and SPIO loading in the micelle core and peptide conjugation at the micelle surface. A scrambled peptide (SP) control was used to investigate the $\alpha_v\beta_6$-specific cell uptake of LCP-encoded MFM. (B) Transmission electron microscopy (TEM) image of a representative MFM sample illustrating the clustering of SPIO nanoparticles (6 nm in diameter) in each MFM particle. (C) Dynamic light scattering analysis of a representative MFM sample (LCP20-MFM, Table 1) for the measurement of MFM size and size distribution in aqueous solution.

Table 1. Physical Characterization of LCP- and SP-Encoded MFM Nanoparticles

				SPIO loading		Doxo loading	
micelles	surface peptide	surface density (%)[a]	size (nm)[b]	LC (%)[c]	LE (%)[d]	LC (%)[c]	LE (%)[d]
LCP20-MFM	RGDLATLRQL	20	48 ± 6	11.6 ± 0.5	77	5.0 ± 0.2	50
LCP40-MFM	RGDLATLRQL	40	60 ± 5	11.9 ± 0.5	79	5.2 ± 0.2	52
SP20-MFM	DALRLQGTLR	20	50 ± 5	11.3 ± 0.5	75	5.4 ± 0.3	54
SP40-MFM	DALRLQGTLR	40	66 ± 5	11.7 ± 0.5	78	5.3 ± 0.3	53
N-MFM	No peptide	0	45 ± 4	11.5 ± 0.5	77	5.2 ± 0.2	52

[a] Molar percentage of Mal-PEG-PLA copolymers conjugated with peptides (HPLC assay shows >95% conjugation efficiency). [b] Hydrodynamic diameter was measured by dynamic light scattering. [c] Loading content (LC) was calculated as the weight percentage of SPIO or Doxo over the total micelle weight. [d] Loading efficiency (LE) was calculated as the percentage of loaded SPIO or Doxo over the original feeding amount. All data were obtained from 5 replicate experiments.

targeting peptides (LCP) and scrambled peptides (SP) were synthesized by solid phase peptide synthesis.[16] Superparamagnetic iron oxide nanoparticles (SPIO) were synthesized following a reported method.[19] The $\alpha_v\beta_6$-expressing H2009 and $\alpha_v\beta_6$-negative H460 human lung cancer cell lines were cultured in DMEM and RPMI medium, respectively, with 5% fetal bovine serum (FBS) at 37 °C in 5% CO_2 atmosphere. All other chemicals and solvents were obtained from Sigma-Aldrich, and used without further purification.

Preparation and Physical Characterization of Peptide-Encoded MFM. LCP (NH_2-RGDLATLRQL-PEG_{11}-Cys) or SP (NH_2-DALRLQGTLR-PEG_{11}-Cys) was synthesized on a Symphony Synthesizer (Rainin Instruments, Protein Technologies, Inc. Woburn, MA) by Fmoc solid phase peptide synthesis.[14] Crude peptides were purified by reverse phase

(19) Sun, S.; Zeng, H.; Robinson, D. B.; Raoux, S.; Rice, P. M.; Wang, S. X.; Li, G. Monodisperse MFe_2O_4 (M = Fe, Co, Mn) nanoparticles. *J. Am. Chem. Soc.* **2004**, *126* (1), 273–279.

HPLC using an Grace Vydac peptide C18 column (250 mm × 21.2 mm, 5 μm). The purified peptides were analyzed by analytical RP-HPLC (Varian, RP-C18 column, 250 mm × 4.6 mm, 5 μm) and were greater than 95% purity. The peptide molecular weights were confirmed by MALDI-MS. LCP- or SP-encoded MFM were prepared following a previously published protocol.[13] Briefly, a mixture of Mal-PEG-PLA and MeO-PEG-PLA (or ^{3}H-labeled polymer) (75% by weight, the molar fraction of Mal-PEG-PLA was controlled at 20% and 40% to yield different surface densities of peptides), Doxo (10%) and SPIO (15%) were first dissolved in THF (1 mL) in a glass vial. Next, the mixture was slowly added into 10 mL of an aqueous solution of 0.05 M HEPES and 0.01 M EDTA under sonication (60 Sonic Dismembrator, Fisher Scientific). LCP or SP peptide was then added into the solution to produce a thiol−maleimide linkage for covalent conjugation of peptides on the micelle surface. After overnight shaking under N_2 at room temperature, the micelle solution was filtered through a Millipore syringe filter (pore diameter 0.45 μm) to remove any large aggregates and further purified by centrifugation dialysis (MW cutoff = 10 kDa, Millipore, MA) to remove any free peptides or drugs. After micelle production, the hydrodynamic diameters of the LCP- or SP-encoded micelles were measured using a Viscotek Dynamic Light Scattering (DLS) instrument (Houston, TX) equipped with a He−Ne laser (λ = 825 nm). Scattered light was collected at 90° and data was analyzed from 10 measurements at 20 °C. Transmission electron microscopy (TEM) was performed at 80 keV using a JEOL 1200 EX instrument (Tokyo, Japan). Each micelle solution was placed on a glow discharged copper grid and allowed to adsorb for 2 min. The excess solution was removed by blotting the grid against a filter paper and dried prior to TEM analysis.

Measurement of Loading Content and Efficiency of Doxo and SPIO. Loading content (LC) was calculated as the percentage of loaded agent (Doxo or SPIO) over the total weight of MFM, and loading efficiency (LE) was calculated as the percentage of loaded agent (Doxo or SPIO) over the original feeding amount of the corresponding agent. Doxo loading was determined by a UV−vis spectrometer (Lambda 20, PerkinElmer, USA). First, micelle solutions were lyophilized and redissolved in a mixture of dichloromethane and DMSO (1:1) under bath sonication for 30 min. The suspending SPIO nanoparticles were removed by centrifugation, and the upper solution was collected to measure the Doxo amount by UV absorbance at 480 nm (ε = 20.6 mL mg^{-1} cm^{-1}). For SPIO loading measurement, peptide-encoded MFMs were lyophilized and dissolved in aqua regia solution for 3 h. The samples were diluted to the appropriate concentrations and ionized using an air/acetylene flame on a Varian SpectrAA 50 spectrometer. The Fe ion concentrations from MFM samples were determined using an established calibration curve based on a Fe standard during each measurement.

Time- and Dose-Dependent Uptake of MFM Nanoparticles in H2009 Lung Cancer Cells. In this series of experiments, we used $\alpha_v\beta_6$-expressing H2009 lung cancer cells to evaluate the effects of peptide surface density, micelle dose and cell incubation time on the uptake of MFM nanoparticles. H2009 cells were grown in 6-well plates and then incubated with ^{3}H-labeled, LCP- or SP-encoded MFM at different micelle doses. At different incubation times, H2009 cells were washed with phosphate-buffered saline (PBS) for 3 times, trypsinized and harvested in PBS. Then the cells were added to the Ready Organic liquid scintillation cocktails for counting. The cell-associated radioactivity, disintegrations per minute (dpm), was measured using a LS60001C scintillation counter (Beckmann, CA) and normalized by the number of cells (i.e., 100,000).

Confocal Laser Scanning Microscopy (CLSM). In this series of experiments, $\alpha_v\beta_6$-expressing H2009 and $\alpha_v\beta_6$-negative H460 lung cancer cells were used to evaluate the cell targeting specificity of LCP-encoded MFM. SP-encoded MFM was used as a control, and the peptide density was controlled at 20% for both MFM formulations. First, H2009 and H460 cells were seeded into 6-well plates with glass bottoms for confocal imaging at a seeding density of 3.0 × 10^5 cells per well. After the cells reached 80% confluence, free Doxo and peptide-encoded MFM were incubated with both cell lines at 4 μM of Doxo concentration for each well. After 2 h of incubation, cells were washed with PBS 3 times and stained with Alexa Fluor 350-conjugated wheat germ agglutinin (Invitrogen, CA) for cell membranes. Cell samples were examined on a Nikon TE2000-E confocal laser scanning microscope (Tokyo, Japan). Alexa Fluor 350 and Doxo were excited at 352 and 485 nm with emissions at 455 and 595 nm, respectively.

Cell Cytotoxicity Studies. The cytotoxicity of free Doxo, N-MFM, LCP- and SP-encoded MFM was evaluated in $\alpha_v\beta_6$-expressing H2009 lung cancer cells. First, H2009 cells were seeded in 96-well plates with a seeding density of 700 cells per well. Cells were maintained in the culture media for 1 day at 37 °C in a humidified atmosphere with 5% CO_2. Then, the cells were treated with free Doxo or MFM samples at different Doxo concentrations. The amount of ATP, which is present only in metabolically active cells, was measured using a luminescent cell viability assay kit (CellTiter-Glo, Promega, WI) after 5 days of treatment. Luminescent signal as produced by the luciferase-catalyzed reaction between luciferin and ATP was recorded using a luminescent counter (Spectra Max M5, Molecular Devices, CA) after 10 min at room temperature. Relative cell viabilities were calculated as the percentage of live cells over the untreated cell control. Standard deviations were obtained from 5 replicates.

Magnetic Resonance Imaging (MRI). The T_2 relaxivity (r_2, Fe mM^{-1} s^{-1}) of the peptide-encoded MFM was measured at 1.41 T using a standard Carr−Purcell−Meiboom−Gill (CPMG) sequence on a Bruker desktop relaxometer (MQ60 model, Ettlingen, Germany). The Fe concentrations in MFM samples were determined on a Varian SpectrAA 50 spectrometer (air/acetylene flame). The T_2 relaxation rates ($1/T_2$, s^{-1}) were plotted as a function of Fe concentrations and the slopes were measured as the T_2 relaxivity for both MFM formulations.

MR imaging of MFM uptake in lung cancer cells was conducted on a 4.7 T horizontal MR scanner (Varian, Palo Alto, CA). H2009 cells were separately seeded on 100 mm diameter cell culture dishes with a seeding density of 1.4×10^6 cells per well. After incubation with LCP- or SP-encoded MFM at different Fe doses for 2 h, cells were washed by PBS three times, harvested and fixed with 2% paraformaldehyde. Then the cells were mixed with 2% agarose in PBS solution (Type VIIA) and transferred into truncated 384 well plates. The cell plates were placed in a 3.8 cm × 5 cm Litz coil (Doty Scientific, Columbia, SC) and T_2-weighted images were acquired with spin echo pulse sequence (TR = 2 s and TE = 60 ms). The MRI signal intensity was normalized to that of untreated cells. Standard deviation was obtained from 5 replicates for each sample. Statistical analysis was applied to all the experiments. The p values were calculated using Student's two-tailed t test for paired comparisons, and $p < 0.05$ is considered statistically significant.

Results

Physical Characterization of Peptide-Encoded MFM. Figure 1A shows the schematic production of LCP- and SP-encoded PEG-PLA (5 kDa−5 kDa) polymeric micelles that were loaded with Doxo and SPIO. Amphiphilic block copolymers of Mal-PEG-PLA and MeO-PEG-PLA were used for micelle formation. Peptides were conjugated to the micelle surface through covalent thiol-maleimide linkages with cysteine-terminated peptides (LCP, NH_2-RGDLATL-RQL-PEG_{11}-Cys; SP, NH_2-DALRLQGTLR-PEG_{11}-Cys). Different molar fractions (i.e., 20% and 40%) of Mal-PEG-PLA were introduced to control the density of peptides (LCP or SP) on the micelle surface (Table 1). Peptide conjugation efficiency from all micelle samples was higher than 95% through the quantification of unreacted peptides by HPLC after surface conjugation. Figure 1B shows the TEM image of a representative MFM sample (20% LCP surface density) where SPIO nanoparticles formed a high density of clusters inside the micelles as previously reported.[20] Dynamic light scattering (DLS) was used to measure the hydrodynamic diameter of the MFM samples. LCP- and SP-encoded MFM nanoparticles showed similar size at the same peptide surface densities (Table 1). For example, at 20% peptide density, the hydrodynamic diameters of LCP- and SP-encoded micelles were 48 ± 6 nm and 50 ± 5 nm in aqueous solution, respectively. At higher peptide density (i.e., 40%), the hydrodynamic diameters of LCP- and SP-encoded micelles were slightly larger at 60 ± 5 nm and 66 ± 5 nm, respectively. However, there was no statistical difference between the LCP- and SP-encoded micelles at the same peptide density ($p > 0.10$).

The loading content (LC) and loading efficiency (LE) of SPIO and Doxo were comparable in all MFM formulations (Table 1). For all five MFM samples, the LC values for SPIO varied between 11% to 12% (theoretical loading content: 15%) with LE values between 75% and 80%. The LC values for Doxo varied between 5.0 and 5.5% (theoretical loading content: 10%) with LE values between 50 and 55%. The higher LE values for SPIO may reflect the more hydrophobic nature of SPIO nanoparticles than Doxo. The comparable loading contents of SPIO and Doxo in all MFM samples allow for the specific examination of peptide type (i.e., LCP vs SP) and peptide density (20% vs 40%) on the targeting efficiency of MFM to lung cancer cells.

Time- and Dose-Dependent Uptake of LCP-Encoded MFM in $\alpha_v\beta_6$-Expressing H2009 Lung Cancer Cells. We systematically investigated the effects of incubation time and micelle dose on the targeting efficiency of LCP-encoded MFM in $\alpha_v\beta_6$-expressing H2009 lung cancer cells. ^{3}H-Labeled MFM were used in these studies. Figure 2A shows the quantitative MFM (20% peptide surface density) uptake in H2009 cells as a function of incubation time. The micelle dose of the LCP20-MFM and SP20-MFM samples was controlled at the same 19.4 μg/mL polymer concentration. Micelle uptake was more rapid with LCP20-MFM than SP20-MFM in the first 2 h and reached a plateau at longer time. At 5 h, the radioactivity reached $7.8 \pm 0.8 \times 10^2$ dpm for LCP20-MFM, approximately 3 times higher than SP20-MFM ($2.5 \pm 0.5 \times 10^2$ dpm, $p < 0.005$).

Figure 2B shows the cell uptake as a function of micelle dose for LCP- and SP-encoded MFM nanoparticles with different peptide densities after 5 h of incubation. For all MFM formulations, higher micelle dose led to increased amount of MFM uptake in H2009 cells as expected. Further examination of the data indicates several trends: first, at the same peptide surface density (i.e., 20% or 40%), LCP-encoded MFM demonstrated higher amount of micelle uptake than SP-encoded MFM at all micelle doses. This is an important illustration of $\alpha_v\beta_6$-dependent targeting specificity by LCP-encoded MFM over the scrambled peptide control. Second, for both LCP- and SP-encoded MFM samples, higher peptide surface density (i.e., 40%) resulted in increased cell uptake than MFM with lower peptide density. Although this is expected from LCP-encoded micelles, the data from SP-encoded MFM suggests that SP peptide may also induce MFM internalization through $\alpha_v\beta_6$-independent mechanisms. The peptides (NH_2-DALR-LQGTLR-$CONH_2$ and NH_2-RGDLATLRQL-$CONH_2$) carry a 2+ charge per peptide at pH 7. The increased peptide density leads to an increased number of positive charges on the MFM surface, which may facilitate the electrostatic interactions with negatively charged cell membranes, and subsequently increase the nonspecific uptake of MFM nanoparticles. Since LCP has the same amino acid composition as SP, presumably the same electrostatic factors would also contribute to the increased MFM uptake with higher LCP density in addition to the $\alpha_v\beta_6$-dependent mechanism. To minimize the nonspecific uptake mechanisms, we chose LCP20-MFM and SP20-MFM for subsequent studies.

(20) Ai, H.; Flask, C.; Weinberg, B. D.; Shuai, X.; Pagel, M. D.; Farrell, D.; Duerk, J.; Gao, J. Magnetite-loaded polymeric micelles as ultrasensitive magnetic-resonance probes. *Adv. Mater.* **2005**, *17*, 1949–1952.

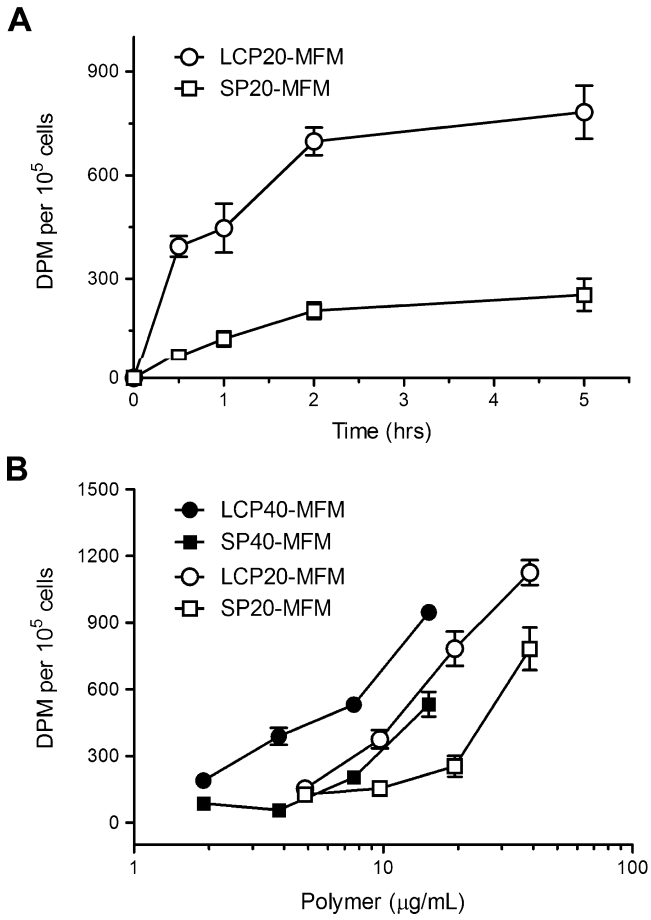

Figure 2. Time- and dose-dependent uptake of peptide-encoded MFM in $\alpha_v\beta_6$-expressing H2009 lung cancer cells. (A) Cell-associated radioactivity (dpm per 10^5 cells) as a function of incubation time after treatment with ^{3}H-labeled LCP20-MFM and SP20-MFM. The MFM dose was kept at 19.4 μg/mL for both MFM samples. (B) Cell uptake of MFM nanomedicine with different peptide encoding and surface density as a function of MFM dose (represented by polymer concentration). The incubation time with H2009 cells was kept at 5 h for all MFM samples. Standard deviation was calculated from 5 replicates for each data point.

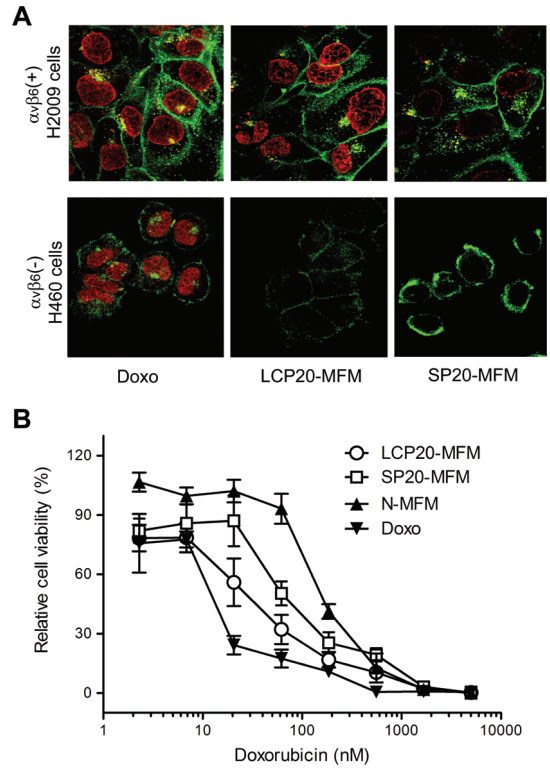

Figure 3. (A) Confocal laser scanning microscopy of Doxo fluorescence in $\alpha_v\beta_6$-expressing H2009 and $\alpha_v\beta_6$-negative H460 cells treated with free Doxo, LCP20-MFM and SP20-MFM. The Doxo concentration was kept at 4 μM for all samples and incubation time at 2 h. Cell membrane was stained with Alexa Fluor 350 and pseudocolored with green. Alexa Fluor 350 and Doxo were excited at 352 and 485 nm with emissions at 455 and 595 nm, respectively. (B) Growth inhibition assay of H2009 cells after treatment with free Doxo, LCP20-MFM, SP20-MFM and N-MFM. Relative cell viability (%) was calculated as the percentage of viable cells after treatment over the untreated cell control. IC_{50} values (Doxo concentration at which the relative cell viability is equal to 50%) were used to compare the different Doxo-containing samples and reported in the text. Standard deviation was obtained from 5 replicates ($n = 5$).

Cell Uptake Study by Confocal Laser Scanning Microscopy. In addition to the radiolabeling experiments, we also used confocal laser scanning microscopy (CLSM) to study the targeting specificity of LCP-encoded micelles to $\alpha_v\beta_6$-expressing H2009 over the $\alpha_v\beta_6$-negative H460 cells (Figure 3A). Free Doxo and SP-encoded MFM were used as controls. The Doxo concentration was controlled at 4 μM for all samples and the incubation time was set at 2 h. From the previous study on the similar PEG-PLA micelle formulation, *in vitro* release rate of Doxo from the micelles appeared to be pH dependent. Due to the ionizable ammonium group on Doxo, Doxo release was faster at acidic environment (e.g., pH 5) than at physiological pH value (7.4).[13] For free Doxo, CLSM images showed rapid nuclear uptake of the drug in both cell lines. Significantly increased amount of LCP20-MFM was observed in $\alpha_v\beta_6$-expressing H2009 lung cancer cells over the $\alpha_v\beta_6$-negative H460 cells. The mean fluorescence intensity (MFI, from an average of 15 cells) was $9.9 \pm 1.3 \times 10^2$ and $4.6 \pm 1.2 \times 10^2$ for H2009 and H460 cells ($p < 0.001$), respectively. Moreover, there was significant increase of LCP20-MFM uptake over SP20-MFM in $\alpha_v\beta_6$-expressing H2009 lung cancer cells. The MFI values were $9.9 \pm 1.3 \times 10^2$ and $5.2 \pm 0.6 \times 10^2$ for LCP20-MFM and SP20-MFM ($p < 0.002$), respectively. The $\alpha_v\beta_6$ specificity for the uptake of LCP-encoded MFM was further demonstrated by a blocking experiment, where a 10-fold molar excess of free LCP peptides was coadministered to H2009 cells and incubated for 2 h. Doxo fluorescence experiment showed that the LCP-encoded MFM had twice as high fluorescence intensity over the blocking control ($p < 0.001$,

data not shown). These results verified the $\alpha_v\beta_6$-dependent specificity for LCP-encoded MFM uptake. Furthermore, the CLSM data demonstrated that Doxo was successfully released from the multifunctional micelles and subsequently accumulated in the nucleus to achieve desirable cell cytotoxicity as previously reported.[13]

$\alpha_v\beta_6$-Dependent Cell Cytotoxicity of Peptide-Encoded MFM. We used an ATP activity assay to evaluate the viability of H2009 cells after incubation with different MFM samples for 5 days. Free Doxo was used as a positive control. Figure 3B shows the relative cell viability as a function of Doxo dose. For each sample, IC_{50} values were determined as the Doxo concentration at which the relative cell viability fell to 50% of the untreated control cells. LCP20-MFM shows significantly lower IC_{50} (28.3 ± 6.4 nM) than SP20-MFM (73.6 ± 6.3 nM, $p < 0.005$), which is consistent with the previous CLSM and radiolabeling experiments that demonstrate $\alpha_v\beta_6$-dependent uptake in H2009 cells. The MFM sample without peptide functionalization (N-MFM) showed the highest IC_{50} value at 125 ± 11 nM, indicating the basal level of MFM toxicity in H2009 cells. Free Doxo presented the most potent cytotoxicity with an IC_{50} of 10.9 ± 5.9 nM due to its lipophilic nature and ease of accumulation in the cell nuclei.

MRI Evaluation of $\alpha_v\beta_6$-Targeting Specificity of LCP-Encoded MFM. Before MRI experiments, we first measured the T_1 and T_2 relaxivities of LCP20-MFM and SP20-MFM samples at 37 °C using a benchtop relaxometer. Figure 4A shows the T_2 relation rates ($1/T_2$, s^{-1}) as a function of Fe concentration (mM). Linear regression analysis yielded a T_2 relaxivity at 407 ± 17 and 493 ± 13 Fe mM^{-1} s^{-1} for LCP20-MFM and SP20-MFM, respectively. T_1 relaxivities of LCP20-MFM and SP20-MFM were 4.2 ± 1.3 and 3.8 ± 1.0 Fe mM^{-1} s^{-1}, respectively. These high T_2 relaxivity values are consistent with our previous report on the clustered SPIO micelle design to achieve high MRI sensitivity.[13,20] The similar T_2 relaxivity values indicate comparable MR relaxation properties of LCP20-MFM and SP20-MFM samples that are intrinsic to the SPIO-clustered micelle design but independent of peptide functionalization on the micelle surface.

To investigate the MRI capability in visualizing the target specificity of MFM nanoparticles, we measured the signal intensity of H2009 cells that were incubated with LCP20-MFM and SP20-MFM samples. A T_2-weighted imaging method (spin echo sequence, TR = 2 s and TE = 60 ms) was employed on a horizontal 4.7 T MRI scanner. Figure 4B shows the MRI images of an H2009 cell suspension in an agarose gel and the relative signal intensity to the untreated control. At different MFM doses (e.g., [Fe] = 0.05, 0.1, and 0.2 mM), significantly darkened MR contrast was observed for LCP20-MFM samples over the SP20-MFM controls ($p < 0.05$ for all comparisons at different [Fe]). Based on the comparable MR relaxation properties of LCP20-MFM and SP20-MFM samples (Figure 4A), the imaging data demonstrate the ability of MRI to differentiate the image contrast due to $\alpha_v\beta_6$-specific uptake of LCP20-MFM over SP20-MFM.

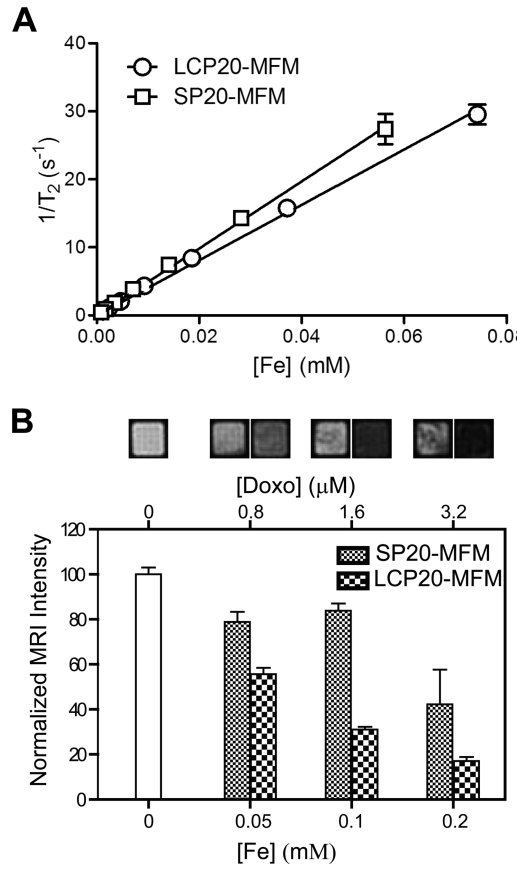

Figure 4. Characterization of MR properties of peptide-encoded MFM and their uptake in $\alpha_v\beta_6$-expressing H2009 cells. (A) T_2 relaxation rates ($1/T_2$, s^{-1}) as a function of Fe concentration (mM) for LCP20-MFM and SP20-MFM at 1.41 T. Linear regression analysis yields the T_2 relaxivity (r_2, Fe mM^{-1} s^{-1}) for both samples. (B) T_2-weighted MRI images and signal intensity of H2009 cells after treatment with LCP20-MFM and SP20-MFM at different micelle doses. H2009 cells were suspended in 2% agarose gel and imaged by a horizontal 4.7T MRI scanner (spin echo sequence, TR = 2 s, TE = 60 ms).

Discussion

Lung carcinomas are generally classified as small-cell (SCLC) or non-small-cell lung carcinomas (NSCLC). The latter category is further subdivided into adenocarcinomas (AD), large-cell carcinomas (LC), and squamous cell carcinomas (SQ). Various genetic changes from normal epithelia are observed in lung cancer, including chromosomal abnormalities, point mutations, and/or DNA methylation.[21,22] These genetic and epigenetic changes can result in changes in protein status including cell surface receptors, leading to

(21) Fong, K. M.; Minna, J. D. Molecular biology of lung cancer: clinical implications. *Clin. Chest Med.* **2002**, *23* (1), 83–101.
(22) Sekido, Y.; Fong, K. M.; Minna, J. D. Molecular genetics of lung cancer. *Annu. Rev. Med.* **2003**, *54*, 73–87.

unique cell surface topographies. Recently, our laboratories have successfully applied phage display panning protocols to identify peptides that mediate binding and uptake into lung cancer cells of different classifications.[15,23] A remarkable feature of the peptides is their cell-specificity (20−1000-fold) for the cell type they are selected against when compared to other cell types. Among the selected peptides, the targeted phage peptide against H2009 cells (H2009.1, also denoted as LCP in this paper) has a broad specificity for NSCLC, binding to 18 out of 39 human NSCLC cell lines tested (data not shown). This peptide binds to H2009 cells 140 times better than a normal bronchial airway epithelial cell line. Recently, integrin $\alpha_v\beta_6$ was identified as the molecular target of the H2009.1 peptide. Expression of $\alpha_v\beta_6$ was examined using a tumor microarray containing tumor samples from 311 lung cancer patients. Its expression is widespread in NSCLC and is correlative with poor patient survival.[17] Interestingly, $\alpha_v\beta_6$ expression is also observed in several other epithelial derived malignancies, including breast cancer, colon cancer, gastric cancer, oral squamous cell cancers, and ovarian cancer.[24−30] Increased expression was correlated with enhanced cell proliferation and migration, and has been suggested to increase the metastatic potential of the tumor.[31,32] The availability of $\alpha_v\beta_6$-targeted and other lung cancer-targeted peptides provides an exciting toolbox to target different lung tumor phenotypes based on the different molecular profiles on lung cancer cells.

The objective of this study is to establish lung cancer-specific multifunctional nanomedicine for targeted therapy of lung cancer. The nanomedicine platform will capitalize on the availability of lung cancer-specific peptides as described above, while achieving an integrated diagnostic and therapeutic (i.e., theranostic) design to allow for the visualization of therapeutic efficacy by noninvasive imaging methods such as MRI. This combination of diagnostic capability with therapeutic intervention is critical to address the challenges of cancer heterogeneity and adaptive resistance. Molecular diagnosis by imaging is important to verify the cancer biomarkers in the tumor tissue and to guide target-specific therapy. Both intra- and intertumor heterogeneity make this a critical consideration for therapeutic design that will go beyond the era of "one-size-fits-all" generic medicine to tumor-specific, personalized medicine. Even after implementing molecular profiling into targeted therapy design, the task of eradicating all cancer cells would not be over. As the tumor inevitably evolves in response to any given therapy, the molecular analysis of the tumor must be quickly repeated and the results used to intelligently modify the targeting strategy for the cancer. Such adaptive targeting strategies may prove essential to address the challenge of adaptive resistance in cancer cells.

The current multifunctional micelles incorporate a lung cancer-targeting peptide, Doxo drug and SPIO contrast agent into one nanoplatform. This prototype system demonstrates consistent $\alpha_v\beta_6$-dependent cellular targeting and nanoparticle uptake, MR contrast and cell cytotoxicity in the cognate lung cancer cells. MRI was chosen as our imaging modality due to its high spatial and temporal resolution and excellent soft tissue contrast. One of the major limitations in MR molecular imaging applications is the inadequate contrast sensitivity of MR probes. For example, traditional T_1-based contrast agents (e.g., Gd-DTPA) have only millimolar (mM) detection levels, which are not sensitive enough for imaging tumor markers at much lower concentrations. Our SPIO-clustered polymeric micelle design has considerably decreased the MR detection limit to subnanomolar concentrations (<nM) of micelles through the increased T_2 relaxivity and high loading of SPIO per micelle particle.[13,20] The T_2 relaxivity (>400 Fe mM^{-1} s^{-1}) as shown in the current MFM design is much higher than that of the commercial Feridex I.V. sample

(23) Brown, K. C. New approaches for cell-specific targeting: identification of cell-selective peptides from combinatorial libraries. *Curr. Opin. Chem. Biol.* **2000**, *4*, 16–21.

(24) Ahmed, N.; Riley, C.; Rice, G. E.; Quinn, M. A.; Baker, M. S. $\alpha_v\beta_6$ Integrin- A marker for the malignant potential of epithelial ovarian cancer. *J. Histochem. Cytochem.* **2002**, *50* (10), 1371–1379.

(25) Arihiro, K.; Kaneko, M.; Fujii, S.; Inai, K.; Yokosaki, Y. Significance of alpha$_9$ beta$_1$ and alpha$_v$ beta$_6$ integrin expression in breast carcinoma. *Breast Cancer* **2000**, *7*, 19–26.

(26) Bates, R. C.; Bellovin, D. I.; Brown, C.; Maynard, E.; Wu, B.; Kawakatsu, H.; Sheppard, D.; Oettgen, P.; Mercurio, A. M. Transcriptional activation of integrin beta6 during the epithelial-mesenchymal transition defines a novel prognostic indicator of aggressive colon carcinoma. *J. Clin. Invest.* **2005**, *115* (2), 339–347.

(27) Breuss, J. M.; Gallo, J.; DeLisser, H. M.; Klimanskaya, I. V.; Folkesson, H. G.; Pittet, J. F.; Nishimura, S. L.; Aldape, K.; Landers, D. V.; Carpenter, W.; et al. Expression of the beta 6 integrin subunit in development, neoplasia and tissue repair suggests a role in epithelial remodeling. *J. Cell Sci.* **1995**, *108* (Part 6), 2241–2251.

(28) Hazelbag, S.; Kenter, G. G.; Gorter, A.; Dreef, E. J.; Koopman, L. A.; Violette, S. M.; Weinreb, P. H.; Fleuren, G. J. Overexpression of the alpha v beta 6 integrin in cervical squamous cell carcinoma is a prognostic factor for decreased survival. *J. Pathol.* **2007**, *212* (3), 316–324.

(29) Jones, J.; Watt, F. M.; Speight, P. M. Changes in the expression of alpha v integrins in oral squamous cell carcinomas. *J. Oral Pathol. Med.* **1997**, *26* (2), 63–68.

(30) Kawashima, A.; Tsugawa, S.; Boku, A.; Kobayashi, M.; Minamoto, T.; Nakanishi, I.; Oda, Y. Expression of alphav integrin family in gastric carcinomas: increased alphavbeta6 is associated with lymph node metastasis. *Pathol. Res. Pract.* **2003**, *199* (2), 57–64.

(31) Agrez, M.; Chen, A.; Cone, R. I.; Pytela, R.; Sheppard, D. The alpha$_v$beta$_6$ integrin promotes proliferation of colon carcinoma cells through a unique region of the beta$_6$ integrin promotes proliferation of colon carcinoma cells through a unique region of the. *J. Cell Biol.* **1994**, *127* (2), 547–556.

(32) Thomas, G. J.; Lewis, M. P.; Whawell, S. A.; Russell, A.; Sheppard, D.; Hart, I. R.; Speight, P. M.; Marshall, J. F. Expression of the $\alpha_v\beta_6$ integrin promotes migration and invasion in squamous carcinoma cells. *J. Invest. Dermatol.* **2001**, *117* (1), 67–73.

(r_2 = 98 Fe mM^{-1} s^{-1}, Berlex Laboratories)[33] and should provide an ultrasensitive nanoprobe for MR detection. Moreover, use of novel imaging methods, such as off-resonance saturation, could further enhance the contrast sensitivity and allow for the *in vivo* imaging of tumor-specific markers in animals.[12]

Although *in vitro* cytotoxicity studies show that free Doxo achieved highest cytotoxicity (i.e., lowest IC_{50} values) in H2009 cells, we anticipate that micelle-delivered drugs will provide better safety and antitumor efficacy *in vivo*. It is well-known that cardiac toxicity is the major morbidity in Doxo-related chemotherapy regimens.[34] Nanoparticle-delivered Doxo (e.g., via liposomes) has shown significantly reduced cardiac toxicity in cancer patients.[35] Preliminary studies in SCID mice showed that free Doxo at 4 mg/kg dose was able to kill all the animals after a single injection; in comparison, all animals survived micelle-delivered Doxo at the same dose after 5 repeated injections (data not shown). In addition to the improved safety, we anticipate that micelle-delivered Doxo will also be able to accumulate more efficiently in solid tumors through the enhanced permeability and retention (EPR) effect[36] that is commonly observed with nanodelivery systems.[37] Moreover, micelle functionalization with LCP peptides will further enhance cell targeting and micelle uptake to improve the therapeutic efficacy of Doxo in lung cancer cells. Current work is in progress to evaluate the *in vivo* MR imaging specificity and antitumor efficacy of LCP-encoded MFM in lung tumor models.

Conclusion

In summary, we report the successful development of a prototype multifunctional micelle (MFM) system where SPIO and Doxo are encapsulated in the micelle core and the micelle surface is functionalized with a lung cancer-targeting peptide. The resulting MFM nanomedicine shows superb T_2 relaxivity (>400 Fe mM^{-1} s^{-1}) for ultrasensitive MR detection. LCP-encoded MFM demonstrate significantly increased cell targeting and micelle uptake in $\alpha_v\beta_6$-expressing H2009 cells over SP-encoded MFM, or in $\alpha_v\beta_6$-negative H460 cells, as verified by ^3H radioactivity measurement, confocal imaging, and MRI. The integrated $\alpha_v\beta_6$-targeting, MRI ultrasensitivity and drug delivery functions in the MFM design open up many exciting opportunities for image-guided, targeted therapy of lung cancer.

Acknowledgment. This research is supported by the National Cancer Institute (R01CA122994 and R01CA129011 to J.G., R01CA106646 to K.C.B. and NCI SPORE P50CA70907 to J.D.M.) and the Welch Foundation (I1622 to K.C.B.). S.-G.Y. is partially supported by a Korean Research Foundation Grant (MOEHRD, KRF-2006-214-E00039). G.H. is supported by a Susan G. Komen foundation postdoctoral fellowship (PDF0707216). C.K. is supported by a DOD Breast Cancer Research Program Multidisciplinary Postdoctoral Award (W81XWH-06-1-0751). MR imaging was facilitated by the NCI SW-SAIR grant (U24 CA126608). This is manuscript CSCN047 from the program in Cell Stress and Cancer Nanomedicine in the Simmons Comprehensive Cancer Center at the University of Texas Southwestern Medical Center at Dallas.

MP9001393

(33) Wang, Y. X.; Hussain, S. M.; Krestin, G. P. Superparamagnetic iron oxide contrast agents: physicochemical characteristics and applications in MR imaging. *Eur. Radiol.* **2001**, *11* (11), 2319–2331.

(34) Buzdar, A. U.; Marcus, C.; Smith, T. L.; Blumenschein, G. R. Early and delayed clinical cardiotoxicity of doxorubicin. *Cancer* **1985**, *55* (12), 2761–2765.

(35) Gabizon, A. A. Pegylated liposomal doxorubicin: metamorphosis of an old drug into a new form of chemotherapy. *Cancer Invest.* **2001**, *19* (4), 424–436.

(36) Maeda, H. The enhanced permeability and retention (EPR) effect in tumor vasculature: the key role of tumor-selective macromolecular drug targeting. *Adv. Enzyme Regul.* **2001**, *41*, 189–207.

(37) Moghimi, S. M.; Hunter, A. C.; Murray, J. C. Long circulating and target-specific nanoparticles: theory to practice. *Pharmacol. Rev.* **2001**, *53*, 283–318.